

**NOVEL SERIES RESONANT HIGH-VOLTAGE DC-DC CONVERTER
TOPOLOGIES FOR X-RAY SYSTEMS**

LEE SZE SING

UNIVERSITI SAINS MALAYSIA

2013

**NOVEL SERIES RESONANT HIGH-VOLTAGE DC-DC CONVERTER
TOPOLOGIES FOR X-RAY SYSTEMS**

by

LEE SZE SING

**Thesis submitted in fulfillment of the requirements
for the degree of
Doctor of Philosophy**

April 2013

ACKNOWLEDGEMENTS

First and foremost, I would like to express my sincere appreciation to my supervisor Dr. Shahid Iqbal for his guidance, encouragement and support. I consider myself lucky and honor to conduct research under his watchful eyes. We have interesting discussions throughout the course of my research. I thank him for his innovative ideas and valuable suggestions, without which I would have not gotten this far.

I am also grateful to my co-supervisor Dr. Mohamad Kamarol who always been supportive, and not to forget his financial assistance for attending several international conferences. Many thanks to the following Power Lab technical staffs, Mohamad Nazir, Ahmad Shaukhi, Jamaluddin and Hairul Nizam for their technical guidance on handling the instruments during my experimental works. I also take this opportunity to thank Mohd Zuber, who helped me a lot in the PCB fabrication for my laboratory prototype.

My thanks to all my teachers and lecturers in primary school, secondary school, matriculation college and university for their willingness to share their knowledge with me and educate me. It is limited space here to put all their names in. I am grateful to lecturers of electrical department, Dr. Dahaman Ishak, Assoc. Prof. Dr. Syafrudin Masri, and Dr. Mohamad Kamarol for their teaching in various subjects in electrical engineering during my undergraduate course. Special gratitude goes to Assoc. Prof. Dr. Soib Taib, who taught me on power electronics during my undergraduate course and guided me very well during my final year project.

I am greatly indebted to my friends, housemates and course mates Chai Wuh Shing, Yew Chuu Tian and Yeong Chee Yan for our talks and laugh and discussions on candidature matters.

On a personal note, I would like to thank my girlfriend Heng Yeh En for her love, encouragement, support and understanding when I had to work instead of spending time with her. I sincerely thank her for being by my side. Hoping that we will explore our great future awaiting us together hand-in-hand.

This thesis is dedicated to my family as well. My parents deserve more thanks than can be put into words. My deepest gratitude goes to my dearest parents, brothers, and sisters for their unfailing care, sacrifice and love. I must say that it was their sincere support that helped me to reach this milestone.

Finally, I would like to acknowledge the Universiti Sains Malaysia for funding me through the Fellowship Scheme for the first five months (August–December 2010). For the remaining months during my doctorate candidature, I am funded by the Malaysian Ministry of Higher Education through the MyBrain 15-MyPhD program. In addition, the research is funded by the following grants: Research University-Postgraduate Research Grant Scheme (RU-PRGS) with grant No. 1001/PELECT/8044048, incentive and short term grant with grant No. 304/PELECT/60311002, and Research University (RU) grant with grant No. RU1001/PELECT/814104, all from Universiti Sains Malaysia.

TABLE OF CONTENTS

	Page
ACKNOWLEDGEMENTS	ii
TABLE OF CONTENTS	iv
LIST OF TABLES	ix
LIST OF FIGURES	x
LIST OF ABBREVIATIONS	xx
LIST OF SYMBOLS	xxii
ABSTRAK	xxv
ABSTRACT	xxvi
CHAPTER 1 – INTRODUCTION	
1.1 Background	1
1.2 Problem Statements	5
1.3 Research Objectives	5
1.4 Thesis Contributions	5
1.5 Thesis Outline	7
CHAPTER 2 – LITERATURE REVIEW	
2.1 Introduction	9
2.2 AC Voltage Controller Based HV Power Supply	9
2.3 PWM Inverter Based HV Power Supply	10
2.4 VM Based HV Power Supply	14
2.5 Resonant Converter Based HV Power Supply	16

2.5.1	Series Resonant HV DC-DC Converter	18
2.5.2	Parallel Resonant HV DC-DC Converter	23
2.5.3	Series-Parallel Resonant HV DC-DC Converter	24
2.6	Comparison Between Resonant Converter Based HV DC-DC Converter	26
2.7	Summary	29

CHAPTER 3 – METHODOLOGY

3.1	Introduction	30
3.2	ZCS-SR Inverter-fed HV DC-DC Converter	31
3.2.1	Topology Description and Principle of Operation	31
3.2.2	Steady-state Analysis	34
3.2.2.1	Modes of Operation	34
3.2.2.2	Mathematical Analysis	38
3.2.3	Output Voltage Control	44
3.2.3.1	Open Loop Control	45
3.2.3.2	Closed Loop Control	48
3.3	ZCS-SR Inverter-fed VM Based HV DC-DC Converter	50
3.3.1	Topology Description and Principle of Operation	51
3.3.2	Steady-state Analysis	53
3.3.3	Output Voltage Control	55
3.4	ZCS-DSR Inverter-fed HV DC-DC Converter	56
3.4.1	Topology Description and Principle of Operation	56
3.4.2	Steady-state Analysis	57
3.4.2.1	Modes of Operation	57

3.4.2.2	Mathematical Analysis	61
3.4.3	Output Voltage Control	73
3.5	ZCS-DSR Inverter-fed VM Based HV DC-DC Converter	74
3.5.1	Topology Description and Principle of Operation	74
3.5.2	Steady-state Analysis	76
3.5.3	Output Voltage Control	79
3.6	Comparison Between Novel Power Converter Topologies	79
3.7	Summary	82
CHAPTER 4 – DESIGN AND IMPLEMENTATION		
4.1	Introduction	84
4.2	Design of Proposed Power Converters	84
4.2.1	Selection of Tank Capacitors	85
4.2.2	Design of HV Transformer	87
4.2.3	Voltage and Current Stress on Circuit Components	91
4.2.4	Design of Inverter and Drive Circuit	92
4.2.5	Implementation of Resonant Tank	96
4.2.6	Implementation of Full-wave Rectifier and VM Circuit	99
4.2.7	Implementation of Load Resistor	103
4.3	Design of Controller	104
4.3.1	Design of Control Signal Generation Circuit	104
4.3.2	Design of Current Sensing Device	110
4.4	Design of PCB	111
4.5	Summary	115

CHAPTER 5 – RESULTS AND DISCUSSION

5.1	Introduction	116
5.2	ZCS-SR Inverter-fed HV DC-DC Converter	117
5.2.1	Simulation Results	117
5.2.2	Experimental Results	122
5.2.2.1	Open Loop Control	123
5.2.2.2	Closed Loop Control	135
5.3	ZCS-SR Inverter-fed VM Based HV DC-DC Converter	140
5.3.1	Simulation Results	140
5.3.2	Experimental Results	146
5.3.2.1	Open Loop Control	146
5.3.2.2	Closed Loop Control	160
5.4	ZCS-DSR Inverter-fed HV DC-DC Converter	165
5.4.1	Simulation Results	165
5.4.2	Experimental Results	168
5.4.2.1	Open Loop Control	169
5.4.2.2	Closed Loop Control	173
5.5	ZCS-DSR Inverter-fed VM Based HV DC-DC Converter	177
5.5.1	Simulation Results	177
5.5.2	Experimental Results	180
5.5.2.1	Open Loop Control	181
5.5.2.2	Closed Loop Control	185
5.6	Verification of Experimental Results	188
5.7	Summary	193

CHAPTER 6 – CONCLUSION AND FUTURE WORK

6.1	Conclusion	196
6.2	Future Work	199

REFERENCES

APPENDICES

LIST OF PUBLICATIONS

LIST OF TABLES

		Page
Table 2.1	Comparison between resonant converter topologies for HV X-ray generator.	27
Table 3.1	Comparisons between the proposed HV dc-dc converter topologies.	80
Table 4.1	Total resonant tank capacitance for 16 combinations of relay state for $C_1=C_2=C_3=C_4=C_0$.	85
Table 4.2	Total resonant tank capacitance for 16 combinations of relay states for $C_1=C_0$, $C_2=2C_0$, $C_3=4C_0$ and $C_4=8C_0$.	86
Table 4.3	Equations of the maximum voltage and current stress on power switches and circuit components.	91
Table 4.4	Maximum voltage and current stress on power switches and circuit components.	92
Table 4.5	Minimum conductor spacing of PCB for various voltage levels (adopted from [83]: IPC-2221A page 43 Table 6-1).	114
Table 5.1	Specifications of the simulation model for both proposed and conventional PFM converter.	117
Table 5.2	Specifications of experimental prototype for both the proposed and conventional PFM converter.	123
Table 5.3	Comparison of transient rise time for different value of output voltage between open loop and closed loop control.	140
Table 5.4	Specifications of simulation model for both the proposed and conventional PFM converter.	141
Table 5.5	Specifications of experimental prototype for both the proposed and conventional PFM converter.	146
Table 5.6	Comparison of transient rise time for different value of output voltage between open loop and closed loop control.	165
Table 5.7	Comparison between experimental and simulation results.	192
Table 5.8	Comparisons between the proposed HV dc-dc converters based on the experimental results	194

LIST OF FIGURES

		Page
Figure 1.1	X-ray tube [3].	3
Figure 1.2	Load ranges of medical-used X-ray HV dc power supply [4]-[7].	4
Figure 2.1	AC voltage controller based HV power supply [13].	10
Figure 2.2	PWM inverter based HV power supply [14], [15].	11
Figure 2.3	Equivalent circuit of the practical HV transformer.	12
Figure 2.4	Modular inverter based HV dc-dc converter [16].	12
Figure 2.5	Circuit operation of the half-wave VM.	15
Figure 2.6	VM based HV dc-dc converter [17].	15
Figure 2.7	Resonant HV dc-dc converter.	16
Figure 2.8	Types of resonant tank circuit [27].	17
Figure 2.9	Series resonant HV dc-dc converter.	18
Figure 2.10	Two full-bridge inverter-fed series resonant HV dc-dc converter with PSM control [45].	21
Figure 2.11	Three-phase series resonant HV dc-dc converter with IVM control [49].	21
Figure 2.12	Parallel resonant HV dc-dc converter.	23
Figure 2.13	Series-Parallel resonant HV dc-dc converter.	25
Figure 3.1	The impedance of series resonant tank as a function of switching frequency ($ Z_L $ is the impedance of resonant inductor, $ Z_C $ is the impedance of resonant capacitor, $ Z_L + Z_C $ is the impedance of the series resonant tank and f_r is the resonant frequency of the series resonant tank.	30
Figure 3.2	Circuit diagram of the proposed ZCS-SR inverter-fed HV dc-dc converter.	32
Figure 3.3	Key steady-state waveforms of the proposed ZCS-SR inverter-fed and ZCS-SR inverter-fed VM based HV dc-	

	dc converter: (a) at minimum total resonant tank capacitance, $C_{T(min)}$, (b) at maximum total resonant tank capacitance, $C_{T(max)}$.	35
Figure 3.4	Equivalent circuit for each mode of operation of the ZCS-SR inverter-fed HV dc-dc converter: (a) Mode 1, (b) Mode 2, (c) Mode 3, (d) Mode 4, and (e) Dead zone.	37
Figure 3.5	Features of the proposed control scheme for ZCS-SR inverter-fed HV dc-dc converter and ZCS-SR inverter-fed VM based HV dc-dc converter.	45
Figure 3.6	The concept of digitally tuned tank capacitance control.	47
Figure 3.7	Overall concept of steady-state output voltage control by digitally tuning tank capacitance and slightly varying pulse frequency.	48
Figure 3.8	The concept of dual-mode frequency modulation and the improvements on transient response.	49
Figure 3.9	Two stages single phase half-wave VM: (a) positive VM, and (b) negative VM.	50
Figure 3.10	Bipolar single phase half-wave VM.	51
Figure 3.11	Circuit diagram of the proposed ZCS-SR inverter-fed VM based HV dc-dc converter.	52
Figure 3.12	Equivalent circuit for each mode of operation of the ZCS-SR inverter-fed VM based HV dc-dc converter: (a) Mode 1, (b) Mode 2, (c) Mode 3, (d) Mode 4, and (e) Dead zone.	55
Figure 3.13	Circuit diagram of the proposed ZCS-DSR inverter-fed HV dc-dc converter.	56
Figure 3.14	Key steady-state waveforms of the proposed ZCS-DSR inverter-fed HV dc-dc converter and ZCS-DSR inverter-fed VM based HV dc-dc converter.	58
Figure 3.15	Equivalent circuit diagram for each modes of operation of the ZCS-DSR inverter-fed HV dc-dc converter: (a) Mode 1, (b) Mode 2, (c) Mode 3, (d) Mode 4, and (e) Dead zone.	61
Figure 3.16	Circuit diagram of the proposed ZCS-DSR inverter-fed VM based HV dc-dc converter.	75

Figure 3.17	Equivalent circuit diagram for each modes of operation of the ZCS-DSR inverter-fed VM based HV dc-dc converter: (a) Mode 1, (b), Mode 2, (c) Mode 3, (d) Mode 4, and (e) Dead zone.	79
Figure 4.1	Implementation of the primary and secondary winding of the HV transformer.	89
Figure 4.2	Photograph of the implemented HV transformer.	89
Figure 4.3	Full-bridge inverter with isolation/drive circuit.	93
Figure 4.4	Photograph of the implemented full-bridge inverter with isolation/drive circuit.	94
Figure 4.5	Half-bridge inverter with isolation/drive circuit.	95
Figure 4.6	Photograph of the implemented half-bridge inverter with isolation/drive circuit and tank capacitors.	96
Figure 4.7	Schematic diagram of the tank capacitors for the proposed ZCS-SR inverter-fed HV dc-dc converter and ZCS-SR inverter-fed VM based HV dc-dc converter.	97
Figure 4.8	Photograph of the implemented tank capacitors and relays for the proposed ZCS-SR inverter-fed HV dc-dc converter and ZCS-SR inverter-fed VM based HV dc-dc converter.	98
Figure 4.9	Schematic diagrams of the full-wave rectifier and VM for the proposed ZCS-SR inverter-fed HV dc-dc converter and ZCS-SR inverter-fed VM based HV dc-dc converter respectively.	99
Figure 4.10	Photograph of the implemented full-wave rectifier for the proposed ZCS-SR inverter-fed HV dc-dc converter.	100
Figure 4.11	Photograph of the implemented four stages bipolar VM for the proposed ZCS-SR inverter-fed VM based HV dc-dc converter.	100
Figure 4.12	Schematic diagrams of two series connected full-wave rectifiers and two series connected 2-stages half-wave VM circuits for the proposed ZCS-DSR inverter-fed HV dc-dc converter and ZCS-DSR inverter-fed VM based HV dc-dc converter respectively.	102
Figure 4.13	Photograph of the implemented two series connected full-wave rectifiers for the proposed ZCS-DSR inverter-fed HV dc-dc converter.	102

Figure 4.14	Photograph of the implemented two series connected 2-stages half-wave VMs for the proposed ZCS-DSR inverter-fed VM based HV dc-dc converter.	103
Figure 4.15	Photograph of the implemented load resistors.	104
Figure 4.16	Control signal generation circuit: (a) Relays control circuit, and (b) Inverter control circuit.	105
Figure 4.17	Photograph of the implemented control signal generation circuits.	106
Figure 4.18	Photograph of the implemented CT.	111
Figure 4.19	Current carrying capacity and sizes of etched external copper conductors for various temperature rises above ambient (adopted from [83]: IPC-2221A page 41 Figure A).	112
Figure 4.20	Conductor width to cross-section relationship for PCB (adopted from [83]: IPC-2221A page 41 Figure B).	113
Figure 5.1	Simulated maximum and minimum output voltage waveforms of the proposed converter.	118
Figure 5.2	Simulated maximum and minimum output voltage waveforms of the conventional PFM converter.	119
Figure 5.3	Simulated transient output voltage waveform of the proposed (yellow trace) and conventional PFM converter (red trace) for an output voltage of 20.2 kV.	120
Figure 5.4	Comparison of simulated voltage ripple between the proposed (yellow trace) and conventional PFM converter (red trace) for an output voltage of 20.2 kV.	121
Figure 5.5	Comparison of simulated resonant current between the proposed (yellow trace) and conventional PFM converter (red trace) for an output voltage of 20.2 kV.	122
Figure 5.6	Experimental waveforms of maximum output voltage, resonant current and gating signals of both the proposed and conventional PFM converter ($f_s = 37$ kHz and $C_T = 320$ nF).	124
Figure 5.7	Experimental waveforms of minimum output voltage, resonant current and gating signals of the proposed converter ($f_s = 25$ kHz and $C_T = 20$ nF).	124

Figure 5.8	Experimental waveforms of minimum output voltage, resonant current and gating signals of the conventional PFM converter ($f_s = 4$ kHz and $C_T = 320$ nF).	125
Figure 5.9	Comparison of output voltage and resonant current waveforms between the proposed and conventional PFM converter for an output voltage of 2.1 kV: (a) proposed converter ($f_s = 25$ kHz and $C_T = 100$ nF), and (b) conventional PFM converter($f_s = 4$ kHz and $C_T = 320$ nF).	126
Figure 5.10	Comparison of voltage ripple between the proposed and conventional PFM converter for an output voltage of 2.1 kV (channel 1 in ac coupling mode): (a) proposed converter ($f_s = 25$ kHz and $C_T = 100$ nF), and (b) conventional PFM converter($f_s = 4$ kHz and $C_T = 320$ nF).	128
Figure 5.11	Comparison of output voltage and resonant current waveforms between the proposed and conventional PFM converter for an output voltage of 4 kV: (a) proposed converter ($f_s = 32$ kHz and $C_T = 200$ nF), and (b) conventional PFM converter($f_s = 12$ kHz and $C_T = 320$ nF).	130
Figure 5.12	Comparison of voltage ripple between the proposed and conventional PFM converter for an output voltage of 4 kV (channel 1 in ac coupling mode): (a) proposed converter ($f_s = 32$ kHz and $C_T = 200$ nF), and (b) conventional PFM converter($f_s = 12$ kHz and $C_T = 320$ nF).	131
Figure 5.13	Percent ripple of output voltage of both the proposed and conventional PFM converter as a function of the output voltage.	132
Figure 5.14	Percent ripple of output voltage of both the proposed and conventional PFM converter as a function of the switching frequency for a load resistance of 400 k Ω .	133
Figure 5.15	Percent ripple of output voltage of both the proposed and conventional PFM converter as a function of the switching frequency for a load resistance of 100 k Ω .	133
Figure 5.16	Efficiency of both the proposed and conventional PFM converter as a function of the output power.	135
Figure 5.17	Transient output voltage waveform of the proposed converter with: (a) open loop control, and (b) closed loop control (for a target output voltage of 0.4 kV).	136

Figure 5.18	Transient output voltage waveform of the proposed converter with: (a) open loop control, and (b) closed loop control (for a target output voltage of 3.25 kV).	138
Figure 5.19	Transient output voltage waveform of the proposed converter with: (a) open loop control, and (b) closed loop control (for a target output voltage of 6.1 kV).	139
Figure 5.20	Simulated maximum and minimum output voltage waveforms for the proposed converter.	141
Figure 5.21	Simulated maximum and minimum output voltage waveforms for the conventional PFM converter.	142
Figure 5.22	Simulated transient output voltage waveforms of the proposed (yellow trace) and conventional PFM converter (red trace) for an output voltage of 19.4 kV.	143
Figure 5.23	Comparison of simulated voltage ripple between the proposed (yellow trace) and conventional PFM converter (red trace) for an output voltage of 19.4 kV.	144
Figure 5.24	Comparison of simulated resonant current between the proposed (yellow trace) and conventional PFM converter (red trace) for an output voltage of 19.4 kV.	145
Figure 5.25	Experimental waveforms of maximum output voltage, resonant current and gating signals of both the proposed and conventional PFM converter ($f_s = 37$ kHz and $C_T = 320$ nF).	147
Figure 5.26	Experimental waveforms of minimum output voltage, resonant current and gating signals of the proposed converter ($f_s = 25$ kHz and $C_T = 20$ nF).	148
Figure 5.27	Experimental waveforms of minimum output voltage, resonant current and gating signals of the conventional PFM converter ($f_s = 4$ kHz and $C_T = 320$ nF).	149
Figure 5.28	Comparison of output voltage and resonant current waveforms between the proposed and conventional PFM converter for an output voltage of 1.6 kV: (a) proposed converter ($f_s = 37$ kHz and $C_T = 40$ nF), and (b) conventional PFM converter($f_s = 4$ kHz and $C_T = 320$ nF).	151
Figure 5.29	Comparison of voltage ripple between the proposed and conventional PFM converter for an output voltage of 1.6 kV (channel 1 in ac coupling mode): (a) proposed converter ($f_s = 37$ kHz and $C_T = 40$ nF), and (b)	

	conventional PFM converter($f_s = 4$ kHz and $C_T = 320$ nF).	152
Figure 5.30	Comparison of output voltage and resonant current waveforms between the proposed and conventional PFM converter for an output voltage of 5 kV: (a) proposed converter ($f_s = 32$ kHz and $C_T = 140$ nF), and (b) conventional PFM converter($f_s = 14$ kHz and $C_T = 320$ nF).	153
Figure 5.31	Comparison of voltage ripple between the proposed and conventional PFM converter for an output voltage of 5 kV (channel 1 in ac coupling mode): (a) proposed converter ($f_s = 32$ kHz and $C_T = 140$ nF), and (b) conventional PFM converter($f_s = 14$ kHz and $C_T = 320$ nF).	154
Figure 5.32	Percent ripple of output voltage of both the proposed and conventional PFM converter as a function of the output voltage.	155
Figure 5.33	Percent ripple of output voltage of both the proposed and conventional PFM converter as a function of the switching frequency for a load resistance of 400 k Ω .	156
Figure 5.34	Percent ripple of output voltage of both the proposed and conventional PFM converter as a function of the switching frequency for a load resistance of 100 k Ω .	157
Figure 5.35	Efficiency of both the proposed and conventional PFM converter as a function of the output power.	158
Figure 5.36	Transient output voltage waveform of the proposed converter with: (a) open loop control, and (b) closed loop control (for a target output voltage of 0.53 kV).	162
Figure 5.37	Transient output voltage waveform of the proposed converter with: (a) open loop control, and (b) closed loop control (for a target output voltage of 5 kV).	163
Figure 5.38	Transient output voltage waveform of the proposed converter with: (a) open loop control, and (b) closed loop control (for a target output voltage of 11.4 kV).	164
Figure 5.39	Simulated maximum ($f_s = 32$ kHz) and minimum ($f_s = 20$ kHz) output voltage waveforms of the proposed converter.	165
Figure 5.40	Simulated maximum output voltage waveform during steady-state of the proposed converter ($f_s = 32$ kHz).	166

Figure 5.41	Simulated minimum output voltage waveform during steady-state of the proposed converter ($f_s = 20$ kHz).	166
Figure 5.42	Simulated resonant inductor current waveforms during steady-state of the proposed converter for maximum output voltage ($f_s = 32$ kHz).	168
Figure 5.43	Simulated resonant inductor current waveforms during steady-state of the proposed converter for minimum output voltage ($f_s = 20$ kHz).	168
Figure 5.44	Experimental waveforms of maximum output voltage, resonant current and gating signal of the proposed converter ($f_s = 32$ kHz).	170
Figure 5.45	Experimental waveform of voltage ripple for maximum output voltage of the proposed converter ($f_s = 32$ kHz).	170
Figure 5.46	Experimental waveforms of minimum output voltage, resonant current and gating signal of the proposed converter ($f_s = 20$ kHz).	171
Figure 5.47	Experimental waveform of voltage ripple for minimum output voltage of the proposed converter ($f_s = 20$ kHz).	171
Figure 5.48	The conventional full-bridge inverter-fed PFM HV dc-dc converter.	173
Figure 5.49	Efficiency of both the proposed and conventional PFM converter as a function of the output power.	173
Figure 5.50	Transient output voltage waveform of the proposed converter with: (a) open loop control, and (b) closed loop control (for a target output voltage of 3.15 kV).	174
Figure 5.51	Transient output voltage waveform of the proposed converter with: (a) open loop control, and (b) closed loop control (for a target output voltage of 2.77 kV).	175
Figure 5.52	Simulated maximum ($f_s = 32$ kHz) and minimum ($f_s = 20$ kHz) output voltage waveforms of the proposed converter.	177
Figure 5.53	Simulated maximum output voltage waveform during steady-state of the proposed converter ($f_s = 32$ kHz).	178
Figure 5.54	Simulated minimum output voltage waveform during steady-state of the proposed converter ($f_s = 20$ kHz).	179

Figure 5.55	Simulated resonant inductor current waveforms during steady-state of the proposed converter for maximum output voltage ($f_s = 32$ kHz).	179
Figure 5.56	Simulated resonant inductor current waveforms during steady-state of the proposed converter for minimum output voltage ($f_s = 20$ kHz).	180
Figure 5.57	Experimental waveforms of maximum output voltage, resonant current and gating signal of the proposed converter ($f_s = 32$ kHz).	181
Figure 5.58	Experimental waveform of voltage ripple for maximum output voltage of the proposed converter ($f_s = 32$ kHz).	182
Figure 5.59	Experimental waveforms of minimum output voltage, resonant current and gating signal of the proposed converter ($f_s = 20$ kHz).	182
Figure 5.60	Experimental waveform of voltage ripple for minimum output voltage of the proposed converter ($f_s = 20$ kHz).	183
Figure 5.61	Efficiency of both the proposed and conventional PFM converter as a function of the output power.	184
Figure 5.62	The conventional full-bridge inverter-fed VM based PFM HV dc-dc converter.	184
Figure 5.63	Transient output voltage waveform of the proposed converter with: (a) open loop control, and (b) closed loop control (for a target output voltage of 4.4 kV).	186
Figure 5.64	Transient output voltage waveform of the proposed converter with: (a) open loop control, and (b) closed loop control (for a target output voltage of 3.25 kV).	187
Figure 5.65	Simulation waveforms of maximum and minimum output voltage of the laboratory prototype for the proposed: (a) ZCS-SR inverter-fed HV dc-dc converter, (b) ZCS-SR inverter-fed VM based HV dc-dc converter, (c) ZCS-DSR inverter-fed HV dc-dc converter, and (d) ZCS-DSR inverter-fed VM based HV dc-dc converter.	189
Figure 5.66	Comparison of rise time between experimental and simulation waveforms for the proposed ZCS-SR inverter-fed HV dc-dc converter at: (a) minimum output voltage and (b) maximum output voltage.	190
Figure 5.67	Comparison of rise time between experimental and simulation waveforms for the proposed ZCS-SR inverter-fed VM based HV dc-dc converter at: (a) minimum	

	output voltage and (b) maximum output voltage.	191
Figure 5.68	Comparison of rise time between experimental and simulation waveforms for the proposed ZCS-DSR inverter-fed HV dc-dc converter at: (a) minimum output voltage and (b) maximum output voltage.	191
Figure 5.69	Comparison of rise time between experimental and simulation waveforms for the proposed ZCS-DSR inverter-fed VM based HV dc-dc converter at: (a) minimum output voltage and (b) maximum output voltage.	192

LIST OF ABBREVIATIONS

AC	Alternating current
AC-DC	Alternating current to direct current
ADC	Analog-to-digital converter
BJT	Bipolar junction transistor
CCM	Continuous conduction mode
CT	Current transformer
DC	Direct current
DC-DC	Direct current to direct current
DCM	Discontinuous conduction mode
ESR	Equivalent series resistance
GTO	Gate turnoff thyristor
HV	High-voltage
IGBT	Insulated gate bipolar transistor
MOSFET	Metal-oxide-semiconductor field-effect transistor
OP-AMP	Operational amplifier
PCB	Printed circuit board
PFC	Power factor correction
PFM	Pulse frequency modulation
PSM	Phase shift modulation
PWM	Pulse width modulation
SCR	Silicon controlled rectifier
VM	Voltage multiplier
ZCS	Zero current switching

ZCS-DSR	Zero current switching - double series resonant
ZCS-SR	Zero current switching - series resonant
ZVS	Zero voltage switching

LIST OF SYMBOLS

A_c	Cross sectional area of ferrite core
B_m	Magnetic flux density
C	Resonant tank capacitor
C_0, C_1, C_2, C_3, C_4	Default, 1 st , 2 nd , 3 rd , 4 th resonant tank capacitor
$C_{B1}, C_{B2}, C_{B3}, C_{B4}$	1 st , 2 nd , 3 rd , 4 th bootstrap capacitor
C_i	i^{th} resonant tank capacitor
C_T	Total resonant tank capacitance
$C_{T(\text{max})}$	Maximum resonant tank capacitance
$C_{T(\text{min})}$	Minimum resonant tank capacitance
D_1, D_2, D_3, D_4	1 st , 2 nd , 3 rd , 4 th antiparallel diode of power switches
$D_{B1}, D_{B2}, D_{B3}, D_{B4}$	1 st , 2 nd , 3 rd , 4 th bootstrap diode
$D_{Z1}, D_{Z2}, D_{Z3}, D_{Z4}$	1 st , 2 nd , 3 rd , 4 th zener diode
f_r	Resonant frequency
$f_{r(\text{min})}$	Minimum resonant frequency
f_s	Switching frequency
$f_{s(\text{max})}$	Maximum switching frequency
$f_{s(\text{min})}$	Minimum switching frequency
f_{start}	Switching frequency during startup
I_{CT-1}	Primary current of current transformer
I_{CT-2}	Secondary current of current transformer
L_S	Leakage inductance of high-voltage transformer
L_{S1}	Leakage inductance of 1 st high-voltage transformer
L_{S2}	Leakage inductance of 2 nd high-voltage transformer

m	Stages of voltage multiplier
m_1	Stages of 1 st voltage multiplier
m_2	Stages of 2 nd voltage multiplier
n	Turns ratio of high-voltage transformer
n_1	Turns ratio of 1 st high-voltage transformer
n_2	Turns ratio of 2 nd high-voltage transformer
n_{CT}	Turns ratio of current transformer
N_p	Primary turns of high-voltage transformer
P_{RCT-2}	Power rating of current transformer
r_1, r_2, r_3, r_4	1 st , 2 nd , 3 rd , 4 th electro-mechanical relay
R_{CT-2}	Load resistor of current transformer
r_i	i^{th} electro-mechanical relay
R_L	Load resistor
S1, S2, S3, S4	1 st , 2 nd , 3 rd , 4 th power switch (IGBT)
T_1	1 st high-voltage transformer
T_2	2 nd high-voltage transformer
T_r	Resonant period
V_1	1 st constant voltage across resonant tank capacitor during dead zone
V_2	2 nd constant voltage across resonant tank capacitor during dead zone
$V_{C(\max)}$	Peak voltage across resonant tank capacitor
V_C'	Constant voltage across resonant tank capacitor during dead zone
V_{CT-2}	Secondary voltage of current transformer
V_{fb}	Feedback voltage

V_{in}	Input voltage
V_{max1}	1 st peak voltage across resonant tank capacitor
V_{max2}	2 nd peak voltage across resonant tank capacitor
V_o	Output voltage
$V_{o(max)}$	Maximum output voltage
$V_{o(min)}$	Minimum output voltage
V_p	Primary voltage of high-voltage transformer
V_r	Reference voltage
Z	Impedance
ω_r	Angular resonant frequency

TOPOLOGI-TOPOLOGI PENUKAR AT-AT VOLTAN TINGGI SALUNAN SIRI YANG BARU UNTUK SISTEM-SISTEM SINAR-X

ABSTRAK

Bekalan kuasa arus terus (AT) voltan tinggi (VT) salunan siri modulasi frekuensi denyut (MFD) konvensional mempunyai batasan kawalan yang terhad pada beban ringan, kehilangan pengaliran yang tinggi, voltan riak keluaran yang besar, sambutan fana yang perlahan dan tekanan arus yang tinggi pada komponen-komponen litar pada frekuensi pensuisan rendah. Tesis ini mencadangkan empat topologi baru bagi penukar AT-AT VT, antaranya berpenyongsang SS-PAS (salunan siri - pensuisan arus sifar), berasaskan pengganda voltan (PV) berpenyongsang SS-PAS, berpenyongsang SSB-PAS (salunan siri berkembar -pensuisan arus sifar) dan berasaskan PV berpenyongsang SSB-PAS. Topologi pertama dan kedua dikawal oleh penalaan digital kapasitan tangki dan perubahan frekuensi denyut dengan operasi dwi-mod. Topologi ketiga dan keempat dikawal oleh MFD dengan operasi dwi-mod. Keberkesanan semua topologi bagi penukar kuasa yang telah dicadangkan dan skim kawalan yang sepadan disahkan oleh keputusan simulasi dan eksperimen. Penukar pertama dan kedua mempunyai prestasi yang lebih baik berbanding dengan penukar MFD konvensional dari segi kawalan voltan keluaran yang lebih luas, peratus riak yang lebih rendah, tekanan arus pada komponen-komponen litar yang rendah dan lebih cekap. Ciri-ciri utama penukar ketiga dan keempat adalah mereka amat berkesan dan mempunyai operasi-operasi litar yang sangat mudah. Antara semua penukar yang dicadangkan, penukar AT-AT VT berasaskan PV berpenyongsang SS-PAS adalah pilihan terbaik untuk sistem-sistem sinar-X bagi kuasa dari 100W hingga 350W. Kecekapan yang diukur pada 100W ialah 87% dan 92% pada 350W.

NOVEL SERIES RESONANT HIGH-VOLTAGE DC-DC CONVERTER TOPOLOGIES FOR X-RAY SYSTEMS

ABSTRACT

Conventional pulse-frequency-modulated (PFM) series resonant high-voltage (HV) direct-current (DC) power supplies have the limitations of poor controllability at light load, high conduction loss, large output voltage ripple, slow transient response and high current stress on circuit components at low switching frequencies. This thesis proposes four novel topologies of HV DC-DC converters, namely, ZCS-SR (zero current switching - series resonant) inverter-fed, ZCS-SR inverter-fed voltage multiplier (VM) based, ZCS-DSR (zero current switching - double series resonant) inverter-fed and ZCS-DSR inverter-fed VM based. First and second topologies are controlled by using digital tuning of tank capacitance and variable pulse frequency with dual-mode operation. Third and fourth topologies are controlled by PFM with dual-mode operation. The effectiveness of all the proposed power converter topologies and corresponding control scheme are verified by simulation and experimental results. First and second converters have superior performances compared to the conventional PFM converter in terms of their wider range of output voltage controllability, lower percent ripple, lower current stress on circuit components and higher efficiency. The main features of third and fourth proposed converters are that they are highly efficient and have very simple circuit operations. Among all the proposed converters, the ZCS-SR inverter-fed VM based HV DC-DC converter is the best choice for X-ray systems with the power range from 100W to 350W. The measured efficiency at 100W is 87% and 92% at 350W.

CHAPTER 1

INTRODUCTION

1.1 Background

The evolution of power electronics commences ever since the solid-state devices were introduced. Such progression in power electronics technology is largely driven by the appearance of gate-controlled power switches starting from the BJTs, MOSFETs to IGBTs. These power switches have gradually taken over more and more of the applications previously dominated by SCRs and GTOs.

Hence, the advent of high power and high frequency switching devices has contributed to the widespread applications of power electronics converters in energy conversion and industrial motion control. In the contemporary day, it is a widely acknowledge fact that the electrical energy needs to be converted to make it suitable for various applications such as active power filters, regulated power supplies, heating and lighting control as well as motor drive applications to name a few.

Some of the applications like the power supplies of household appliances have grown and reached their maturity rapidly in recent years. However, the HV dc power supply is an exception. There are less novelty and contribution found in the HV dc power supply. In that case, the designing of power converters and their corresponding control schemes to produce HV in kilo-volt range remains as a challenging task.

There are numerous applications of HV dc power supplies such as lasers, accelerators, ultra-high voltage electron microscopes, and X-ray power generators. However, the design and development of HV dc X-ray power supplies, especially for medical imaging applications, are the most critical. This is because medical imaging HV power supply has certain characteristics beyond a regular power supply to meet the standards necessary for hospital use. It must meet stringent safety specifications with respect to isolation in order that patients and medical staff are protected from the risk of electric shock. The safety guidelines for medical imaging power supply are given by International Electrotechnical Commission (IEC) standard 60601-1. This standard emphasizes on protection against electric shock and provides requirements for clearance, isolation and leakage current.

In addition, X-ray medical imaging power supply must deliver the specified electrical performance to produce optimum amount of X-ray for diagnosing different parts of human body. This is crucial because the radiation particles of X-ray have the ionization capability and hence they would damage the human body when used in high doses [1]. The X-ray generation is controlled by HV that applied across the anode and cathode of X-ray tube.

The X-ray tube as shown in Figure 1.1 is the key component that used to produce X-ray. It consists of a vacuum tube, an anode plate, a cathode filament, a heater power supply and a HV dc power supply [2], [3]. When bring into operation, the heater power supply boils off the electrons from cathode filament. When HV is applied across the anode and cathode terminal, the free electrons leave cathode and

accelerated towards the anode plate. On impact with the anode plate, X-ray which is emitted as the kinetic energy of the electrons is then converted into radiation.

Since the X-ray radiated energy is proportional to the HV applied across the anode and cathode of the X-ray tube, the HV dc power supply plays an important role in controlling the X-ray generation for different applications. Figure 1.2 shows the load ranges of medical used X-ray HV dc power supply [4]-[7]. Tube voltage is the potential different between anode and cathode of the X-ray tube, measured in kilo-volts (kV). On the other hand, the tube current which is measured in milli-amperes (mA) represents the rate of electron accelerated from cathode to anode.

As a matter of fact, the quality of photographic image in medical imaging depends on the X-ray radiated energy which is proportional to the tube voltage [4]-[7]. Specifically, diagnosing different parts of the body requires different level of voltage. For instance, the denser body parts like bone are diagnosed under higher tube voltage, whereas the soft organ tissues require only a relatively lower HV [8], [9]. In this context, a wide range of tube voltage becomes essential. Generally, the voltage across the X-ray tube is set to a value between 20 to 150 kV, depending on the type of application, while the current is varied from 0.5 to 1250 mA [4]-[7].

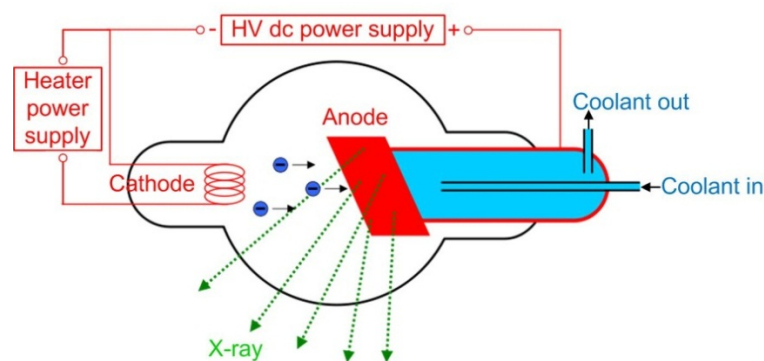


Figure 1.1: X-ray tube [3].

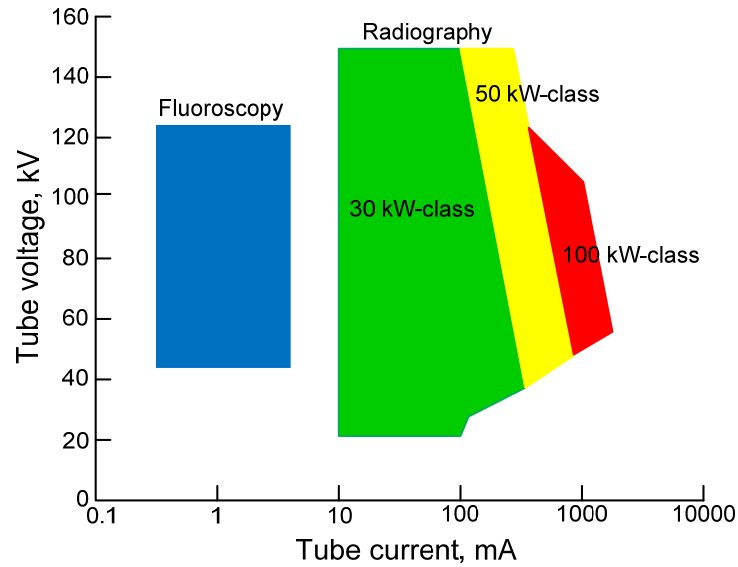


Figure 1.2: Load ranges of medical-used X-ray HV dc power supply [4]-[7].

The HV dc power supply is required to have low voltage ripple and fast transient response. High voltage ripple is not desirable, because it lowers the contrast of photographic X-ray image [10]. Furthermore, the output voltage is required to rise rapidly and reached the steady-state within short interval of time without overshoot to avoid any noise or defect in the image [11], [12]. Essentially, the acceptable rise time is approximately 10 ms or less [12]. To sum up, the HV dc power supply of the X-ray systems is required to provide a wide range of output voltage with low voltage ripple, fast transient rise time and achieve high efficiency.

This thesis introduces new HV dc-dc converter topologies and their control schemes for the application in X-ray generator. When compared with the conventional HV dc-dc converter, the proposed new topologies and control schemes are proved to have better performance in terms of their output voltage controllability, percent ripple, current stress, transient response and efficiency. The contributions are presented and elaborated in the succeeding five chapters.

1.2 Problem Statements

Conventionally, the full-bridge inverter-fed series resonant HV dc-dc converter for X-ray systems is controlled by PFM. To regulate the output voltage over a wide range in light load condition, a wide range of frequency variation is required. This control scheme however has problem of high percent ripple at desired low output voltage. This is because the output ripple increases when the converter is operating at lower switching frequency. In addition, the series resonant HV dc-dc converter also suffers from the slow transient response at low switching frequency. Furthermore, it has low efficiency at low output voltage due to high current stress and hence high conduction loss.

1.3 Research Objectives

The main objectives of this research are:

- To introduce new topology of the series resonant HV dc-dc converter with wide range of output voltage controllability.
- To reduce ripple of output voltage and current stress on circuit components of the series resonant HV dc-dc converter.
- To improve the transient response of output voltage of the series resonant HV dc-dc converter.
- To improve the power efficiency of the series resonant HV dc-dc converter.

1.4 Thesis Contributions

This thesis contributes to the methodology, design and implementation of novel series resonant HV dc-dc converter topologies and their control schemes. The

research proposes four novel HV dc-dc converter topologies which are capable of enhancing the performance of the conventional HV power supply for X-ray systems.

Four novel converter topologies are ZCS-SR inverter-fed HV dc-dc converter, ZCS-SR inverter-fed VM based HV dc-dc converter, ZCS-DSR inverter-fed HV dc-dc converter, and ZCS-DSR inverter-fed VM based HV dc-dc converter. Moreover, this research proposes two control schemes.

Firstly, a digitally tuned tank capacitance and slightly varied pulse frequency with dual-mode operation is proposed for controlling ZCS-SR inverter-fed HV dc-dc converter and ZCS-SR inverter-fed VM based HV dc-dc converter. For the ZCS-DSR inverter-fed HV dc-dc converter and ZCS-DSR inverter-fed VM based HV dc-dc converter, the control scheme is PFM with dual-mode operation.

The design and implementation of 100 W laboratory prototypes of the proposed ZCS-SR inverter-fed HV dc-dc converter, ZCS-DSR inverter-fed HV dc-dc converter, ZCS-DSR inverter-fed VM based HV dc-dc converter, and 350 W laboratory prototype of the proposed ZCS-SR inverter-fed VM based HV dc-dc converter are parts of the contribution of this research. It includes the designing of control circuit and main power circuit as well as their implementations on PCB. The feasibility of the proposed converters is verified through simulations using the OrCAD PSpice and experimental testing upon the laboratory prototypes. The performances of the proposed converters and the conventional PFM converter are taken into comparison.

1.5 Thesis Outline

Chapter 1 presents the introduction of the thesis. The problems related to the design of the HV power supply are discussed. The motive of this thesis is presented and the objectives are given. At the end of this chapter, the thesis outline is shown to briefly discuss the contents of each succeeding chapters.

Chapter 2 reviews the past research work done in HV dc power supply for X-ray systems. All the relevant topologies regarding to the X-ray generator, whether it is the earliest design or the latest design of resonant converter contributed by the researchers worldwide are presented. In recent years, there are three types of resonant topologies have been proposed; they are the series, parallel, and series-parallel resonant HV dc-dc converter. The advantages and drawbacks of each resonant topology are taken into comparison.

Chapter 3 proposes four novel series resonant HV dc-dc converter topologies for X-ray systems. First, the ZCS-SR inverter-fed HV dc-dc converter is discussed. A new method to control the output voltage of this dc-dc converter over a wide range is presented. It is done by digitally tuning tank capacitance and slightly varying pulse frequency with dual-mode operation. The improvements on the first topology are discussed. This improved topology is named as ZCS-SR inverter-fed VM based HV dc-dc converter. Another two topologies which require only two power switches and simple circuit operation are proposed. They are the ZCS-DSR inverter-fed HV dc-dc converter and ZCS-DSR inverter-fed VM based HV dc-dc converter. These two topologies are controlled by PFM with dual mode operation. At the end of this

chapter, all four novel topologies are summarized and compared. The applications of each novel converter topology in X-ray systems are discussed.

Chapter 4 emphasizes the design and implementations of the proposed converters. The design procedures for both the power and control circuit are clarified. The components selection methods, design and implementations of low power laboratory prototypes are the important issues to be discussed in this chapter.

Chapter 5 discusses the simulation and experimental results of the proposed converters. The performances of all four HV dc-dc converter topologies proposed in chapter 3 are evaluated. The simulation and experimental results in open loop control are presented to validate their output voltage control range, percent ripple, and efficiency. Moreover, the comparison between the proposed converters and the conventional PFM converter are given. To evaluate the transient response of the proposed converters, the experimental results in closed loop control are also presented and discussed. Finally, the features of each converter proposed are taken into consideration based on their simulation and experimental results.

Chapter 6 concludes the thesis based on the research findings that have been presented earlier. It discusses the achievements of the research objective and quality of the proposed converters for X-ray systems. Finally, it suggests the potential improvements in the future.

CHAPTER 2

LITERATURE REVIEW

2.1 Introduction

This chapter reviews the HV dc power supply technology for the X-ray systems. All topologies from the earliest design to the recently proposed resonant converters are presented. The advantages and drawbacks of each converter topologies are discussed.

2.2 AC Voltage Controller Based HV Power Supply

Figure 2.1 shows the earliest design of the HV power supply for X-ray generator. In this topology, an auto-transformer is used to regulate the output voltage. The primary winding of the auto-transformer is connected to the line voltage while the secondary winding is switchable to different taps of voltage level. Two thyristors are connected at the secondary winding of the auto-transformer as power switch to control the operation of the power supply. A HV transformer is used to boost the voltage prior to rectification by a full-wave rectifier and supply to the X-ray tube.

This topology has several disadvantages which are undesirable for X-ray application. Although the auto-transformer is able to control the output voltage over a wide range, the accuracy of output voltage is poor. This is because the secondary voltage of the auto-transformer is switched to different voltage level instead of smooth voltage variation. Moreover, the output voltage ripple is very large and the transient rise time is very long because the topology is operating at line frequency of

50/60 Hz. Low operating frequency also reduces the power density of HV transformer, and hence it is bulky and heavy.

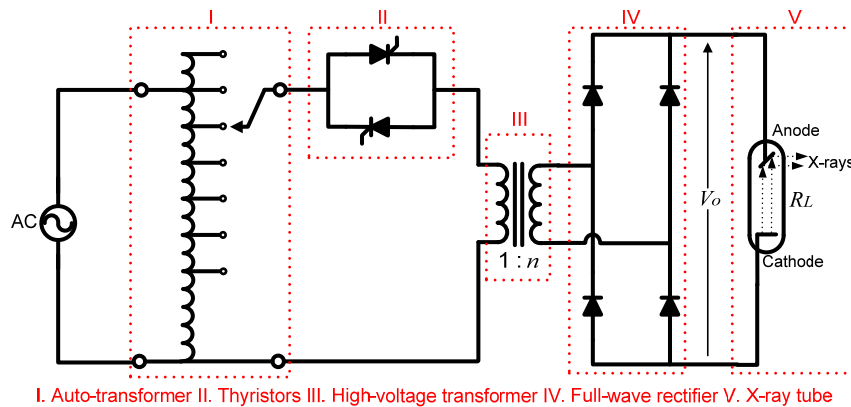


Figure 2.1: AC voltage controller based HV power supply [13].

2.3 PWM Inverter Based HV Power Supply

The low accuracy of output voltage control, high voltage ripple and slow transient response in the aforementioned power topology are highly undesirable for X-ray systems. To lessen these problems, authors in [14], [15] proposed a PWM inverter based HV power supply as shown in Figure 2.2.

In this topology, the line voltage is rectified by a full-wave rectifier with a filter capacitor to produce a stable dc voltage. This dc voltage is then processed by a dc-dc converter to boost up the voltage to a desired value. This dc-dc converter consists of several parts, namely a full-bridge inverter, a high frequency HV transformer, a HV full-wave rectifier and a filter capacitor.

The full-bridge inverter converts dc to ac voltage. The ac voltage produced by the full-bridge inverter is in the form of square wave and having the same frequency with the operating frequency of the inverter. A high frequency transformer with high turns ratio is employed to boost up the ac voltage to kilo-volt range in order to

adapted in the X-ray application. The high ac voltage on secondary is then rectified by a HV full-wave rectifier and filtered through a capacitor before being supplied to the X-ray tube.

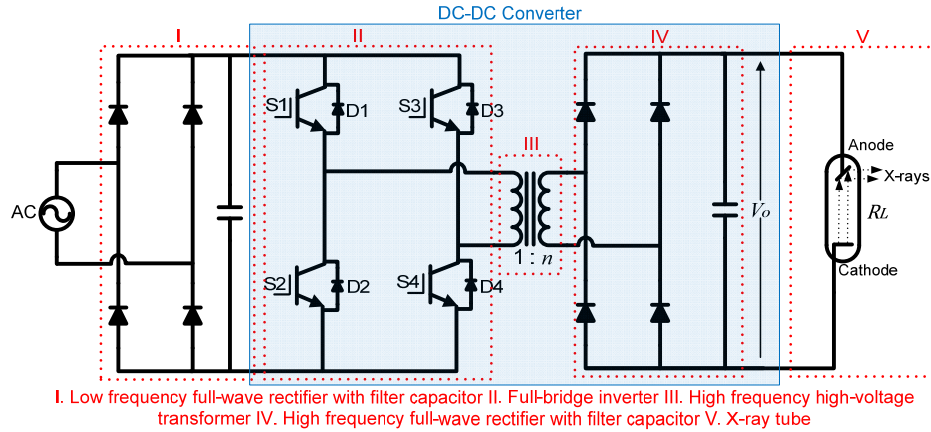


Figure 2.2: PWM inverter based HV power supply [14], [15].

In this topology, the output voltage is controlled by PWM in full-bridge inverter. The full-bridge inverter is operating at high and fixed frequency with variable duty cycle. Higher duty cycle produces higher output voltage and vice versa. By adjusting the duty cycle of switching signals, the output voltage can be controlled accurately. Moreover, high operating frequency reduces the voltage ripple and the size of the system as well.

However, this topology suffers from several drawbacks. The HV transformer used is not ideal and hence affects the performance of the topology. Figure 2.3 shows the equivalent circuit of a practical HV transformer. The high insulation requirement between the primary and secondary winding reduces the magnetic coupling and consequently produces leakage inductance. Moreover, the large number of secondary turns produces significant parasitic capacitance.

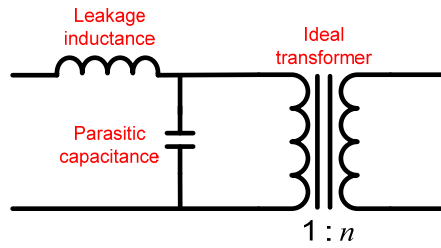


Figure 2.3: Equivalent circuit of the practical HV transformer.

The leakage inductance and parasitic capacitance cause voltage spikes and current spikes respectively. In addition, the leakage inductance slows down the current that flowing through the inverter switches. It also decreases the dynamic response of the output voltage and restricts the operating frequency of the full-bridge inverter to only several hundred hertz [13]. Furthermore, this topology operates in hard switching which reduces the efficiency of the system and causes the switches to heat up.

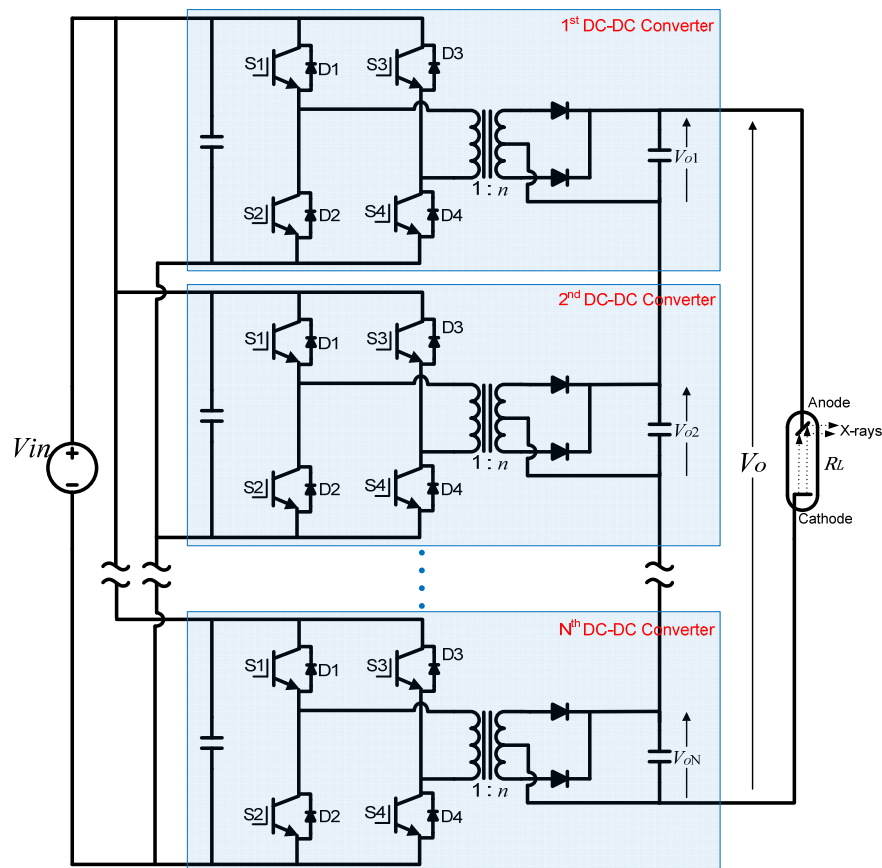


Figure 2.4: Modular inverter based HV dc-dc converter [16].

To reduce the aforementioned parasitic elements, authors in [16] proposed a modular inverter based dc-dc converter as shown in Figure 2.4. In this topology, multiple modules of PWM inverter based dc-dc converter are utilized. The inputs of all these dc-dc converter modules are connected in parallel and they shared a single dc source. Their outputs are connected in series, so that all the output voltages are aggregated before being supplied to the X-ray tube. This topology not only reduces the turns ratio of HV transformer in each module, but also reduces the leakage inductance and parasitic capacitance as well. It also further decreases the voltage rating of the output diodes and current stress on switches.

This topology has numerous drawbacks. The parasitic elements are only reduced but not completely removed. Moreover, as the output of each module is connected in series, the output voltage of each module might not be equivalent. Under this condition, the voltage stresses on each module are unequal. Therefore, in the module with the highest output voltage, the voltage stresses on the circuit components might exceed the rated voltage and causes the entire system failure.

To solve the output voltage balancing problem in each module, a very complicated closed loop control strategy is required. This topology requires high number of switches, HV transformers and diodes, which increase the cost and make the system bulkier. Greater number of switches indicates larger heat sink is in demand compared to the single dc-dc converter module in Figure 2.2. Each switch release heat to surrounding and cause the rapid temperature rise within the modules. Therefore, an efficient cooling system is compulsory to reduce the temperature and avoid the malfunctioning of the HV power supply resulting from overheating.

2.4 VM Based HV Power Supply

Cockcroft-Walton VM is a circuit consists of capacitors and diodes which intended to produce high dc voltage from low ac voltage. It was invented by physicists John Douglas Cockcroft and Ernest Thomas Sinton Walton in 1932. Figure 2.5 shows the two stages single phase half-wave VM. The operations of the VM in Figure 2.5 are presented as below:

1. During the negative cycle of input voltage, diode $D1'$ turns on and $C1'$ is charged to the peak of input voltage, E .
2. During the positive cycle of input voltage, $D2'$ turns on and the input voltage adds arithmetically to the existing voltage across $C1'$. Hence, the capacitor $C1''$ is charged to twice the peak of input voltage, $2E$.
3. During the negative cycle of the input voltage, $D3'$ turns on and the voltage across $C2'$ is equals to the sum of input voltage and voltage across $C1''$ minus voltage across $C1'$. The capacitor $C2'$ is charged to twice the peak of input voltage, $2E$.
4. During the positive cycle of input voltage, $D4'$ turns on. The input voltage, voltage across $C1'$ and $C2'$ are added arithmetically. The effective voltage across $C2''$ is obtained by subtracting the aforementioned sum voltages by the voltage across $C1''$. Hence, the capacitor $C2''$ is charged to twice the peak of input voltage, $2E$.

It is noteworthy that, each single stage of VM produces twice the peak of input voltage. Therefore, authors in [17] replaced the full-wave rectifier in Figure 2.2 with a VM circuit. The resultant circuit diagram of the power converter is shown in Figure 2.6.

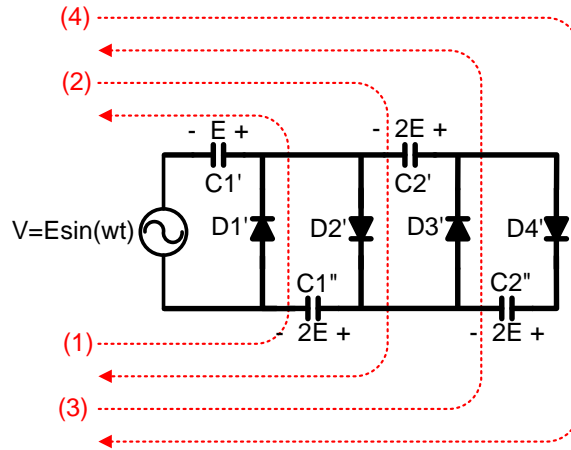


Figure 2.5: Circuit operation of the half-wave VM.

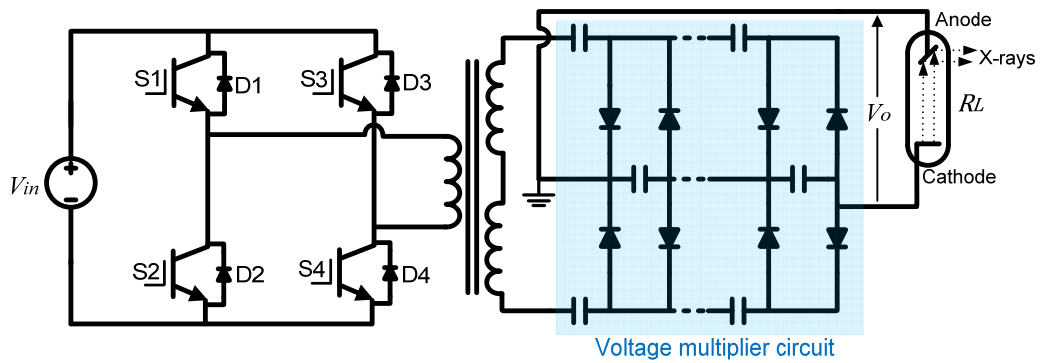


Figure 2.6: VM based HV dc-dc converter [17].

As the VM circuit has the voltage boosting capability, connecting it at the secondary of HV transformer reduces the transformer turns ratio. Hence, the parasitic elements of the HV transformer are reduced. However, the rise time of the VM is proportional to the number of stages. Although deploying of high number of VM stages can reduce the parasitic elements significantly, it causes slow transient response in the power converter. Lengthy rise time of output voltage is undesirable for medical X-ray imaging application. Therefore, authors in [17] proposed only two stages of VM circuit for X-ray generator. In short, this topology can only lessen the effect of parasitic elements but not eradicating them.

2.5 Resonant Converter Based HV Power Supply

An alternative approach to cope with the parasitic elements of HV transformer is to design new topologies of the dc-dc converter which is capable to absorb the non-idealities of HV transformer as useful elements. For this purpose, authors in [18], [19] proposed resonant HV dc-dc converter as shown in Figure 2.7.

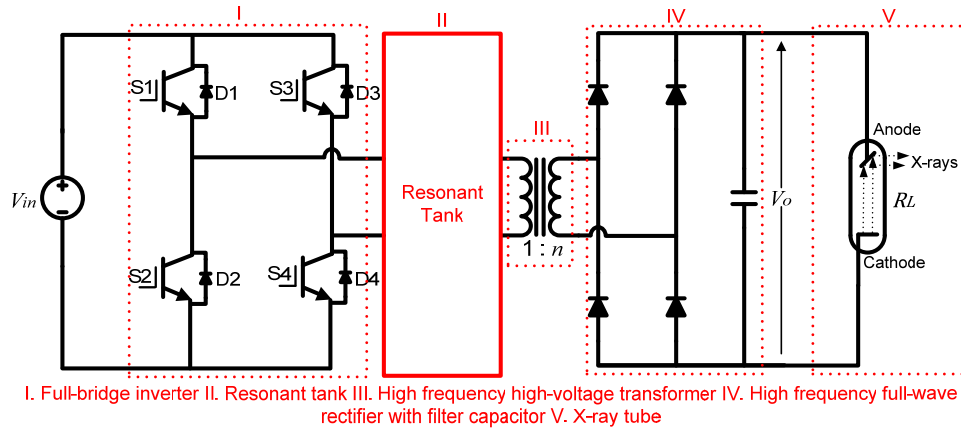


Figure 2.7: Resonant HV dc-dc converter.

Similar to the PWM inverter based dc-dc converter, this topology consists of a full-bridge inverter, a HV transformer, and a HV full-wave rectifier with filter capacitor. Its only difference is that it has an additional resonant tank connected between the full-bridge inverter and HV transformer. The designated resonant tank plays an important role in storing and releasing of energy during operation and therefore causes the current to flow in sinusoidal profile. When high frequency ac voltage in the form of square wave produced by the full-bridge inverter is applied across the resonant tank, the current rings in a piecewise sinusoidal fashion [19].

Exploiting of resonance phenomena in this topology has numerous advantages, namely, low switching loss as the soft switching in inverter switches is achievable, low electromagnetic interference, voltage/current spikes are avoided, and

higher operating frequency, which consequently increases the power density of converter [20]-[22]. Therefore, this topology reduces the size of converter and greatly improves the efficiency [23], [24].

In the broader perspective, there are three types of resonant tank circuit to be employed in this resonant HV dc-dc converter. They are series resonant, parallel resonant and series-parallel resonant tank [25], [26]. Their distinctive concepts are schematically depicted in Figure 2.8.

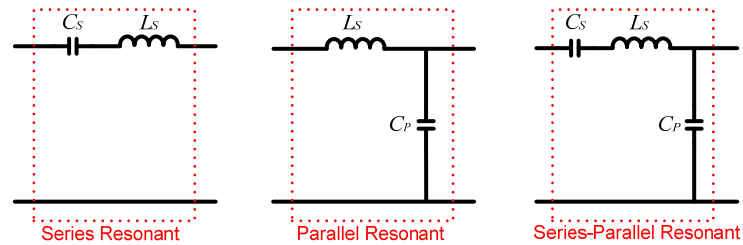


Figure 2.8: Types of resonant tank circuit [27].

In series resonant tank, the tank inductor and capacitor are connected in series. This sort of resonant tank allows the leakage inductance of HV transformer to be absorbed into the topology as long as there is an externally connected series tank capacitor. As for parallel resonant tank, the resonant tank is connected in parallel to the tank capacitor. Since the tank inductor and capacitor are connected exactly the same as the parasitic elements of HV transformer (Figure 2.3), both the leakage inductance and parasitic capacitance are absorbed into the topology. Series-parallel resonant tank is a hybrid of series and parallel resonant tank. In this resonant tank, both leakage inductance and parasitic capacitance of HV transformer are absorbed into the topology once that a series tank capacitor is externally connected.

2.5.1 Series Resonant HV DC-DC Converter

The series resonant HV dc-dc converter as illustrated in Figure 2.9 is the most popular topology for X-ray generator application [28]. The series resonant capacitor in this topology has the ability to block the dc components on the primary side of HV transformer and prevents the transformer saturation [29], [30]. Since the resonant tank is connected in series with the primary of HV transformer, it will limit the current flow through the inverter once that the primary of HV transformer is shorted accidentally and hence provides overload protection as well [26].

Typically, this topology possesses an advantage over other types of resonant converters in such a way that the resonant current is proportional to the load current [26]. As the resonant current decreases with accordance to the reduction in output load, the conduction loss is also reduced at light load condition. Therefore, the efficiency of this topology remains high throughout a wide range of load variation [31]. However, its poor output voltage controllability at light load condition renders it a less satisfactory option to be put into implementation [26], [32], [33].

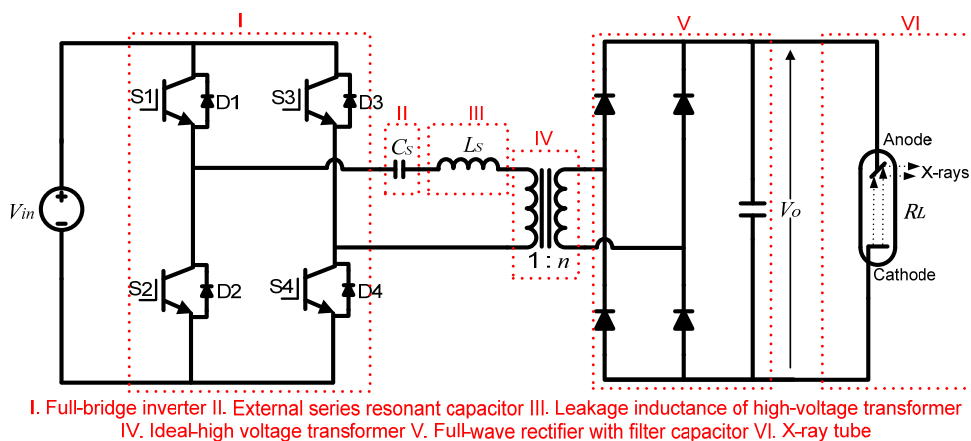


Figure 2.9: Series resonant HV dc-dc converter.

Conventionally, the series resonant HV dc-dc converter for X-ray generator is controlled by PFM [34]. By controlling the frequency of the full-bridge inverter, the output voltage can be regulated. Its operating frequency determines the conduction mode of the converter. When the switching frequency is more than half of resonant frequency, the converter is operating in CCM. On the other hand, the resonant current is discontinuous (DCM) when the switching frequency is less than half of resonant frequency [35], [36].

In CCM, the full-bridge inverter is unable to operate in soft switching condition all the time. When the switching frequency is below the resonant frequency, all the inverter switches achieve soft switching only at the time that they are turn off [27]. On the contrary, when the switching frequency is above resonant frequency, all the inverter switches achieve soft switching only at the time that they are turn on [27], [37].

Authors in [38]-[40] proposed constant on-time PFM to operate the converter in DCM. As the resonant current is discontinuous, all inverter switches are turned on under ZCS condition. They are turn off when the resonant current is flowing in the reversed direction through the anti-parallel diode. In that case, all the switches are turned off under ZCS and ZVS condition [41], [42]. Therefore, operating in DCM has merits of negligible switching loss and hence higher efficiency compared with CCM.

PFM has a disadvantage of wide variation of switching frequency is required in regulating the output voltage, especially at light load condition [43]. At low

switching frequency, the output ripple is extremely large and the transient response is slow, which is undesirable in X-ray application [44], [45]. Having known the problems of wide range frequency variation in PFM, some types of fixed-frequency control strategies have been proposed [46].

Authors in [47] proposed a PSM with the full-bridge inverter operates at the fixed-frequency above resonance. By shifting the phase of switching signals for second leg (S3 and S4) of the full-bridge inverter, the output voltage can be regulated. Higher phase shift results in lower output voltage and vice versa. However, this control scheme does not resolve the problem of controllability at light load. At the desired low output load, the range of output voltage produced is very narrow [37]. Moreover, operating the full-bridge inverter above resonance has a disadvantage of hard switching on inverter switches during turn off.

By using the same control approach as PSM, a new series resonant HV dc-dc converter topology is proposed by authors in [45] as shown in Figure 2.10. In this converter, the inputs of two full-bridge inverters are connected in parallel and they share the same dc source. In contrast, the output voltages of both series resonant inverters are boosted and combined through VM circuit. The output voltage is controlled by varying the phase-shift between the output voltages of both the full-bridge inverters. The main drawbacks of this topology include the constrained of control range in light load condition in addition to its inability to achieve soft switching throughout the entire control range. This topology also has complicated control scheme and it requires large number of switches.

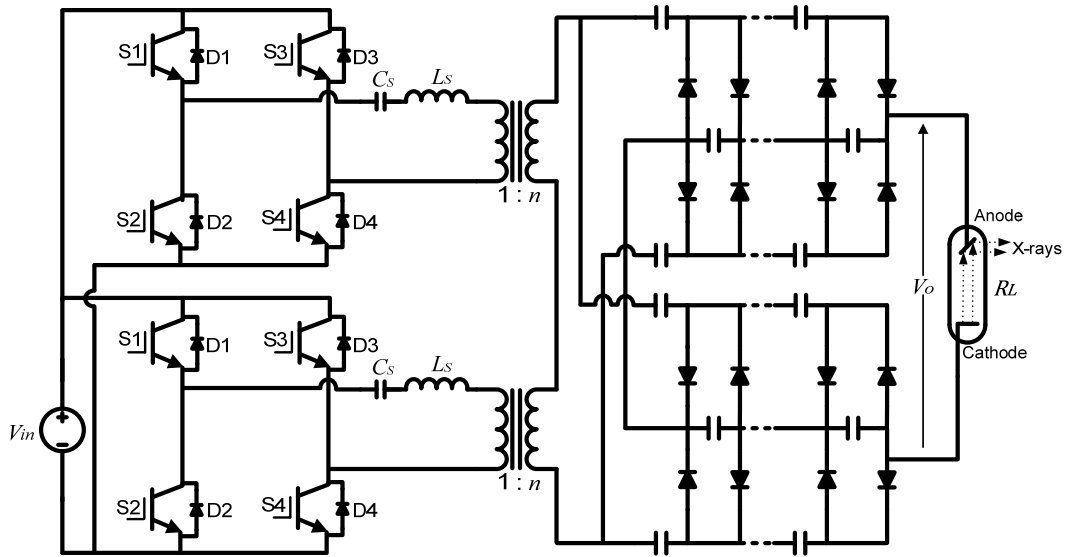


Figure 2.10: Two full-bridge inverter-fed series resonant HV dc-dc converter with PSM control [45].

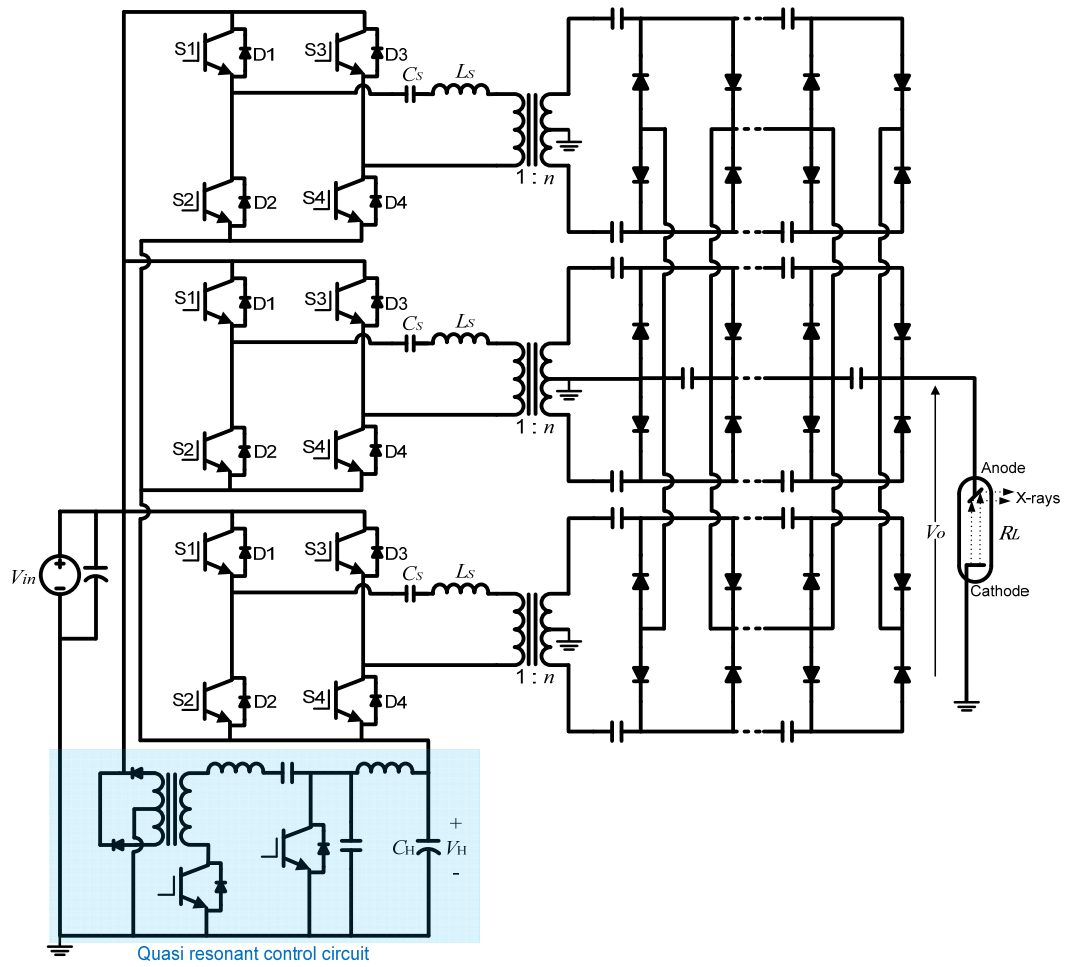


Figure 2.11: Three-phase series resonant HV dc-dc converter with IVM control [49].

Another control scheme, which called the input-voltage-modulation (IVM), was proposed by authors in [48], [49]. This control scheme operates the series resonant HV dc-dc converter in DCM to eliminate switching loss of all switches during both turn on and off condition. The three phase series resonant converter operate with this control scheme is illustrated in Figure 2.11.

The three-phase series resonant converter comprised of three sets of full-bridge inverter in which designated to energize three series resonant tanks. The full-bridge inverters used in this topology operate with a phase shift difference of 120° . The output voltages of each series resonant converter are boosted and combined through a three-phase VM circuit.

The output voltage of the converter is regulated by varying the magnitude of input voltage across the full-bridge inverter, which can be done by adding a quasi-resonant control circuit at the lower arm of the inverter input. This control circuit acts like a dc voltage controller. This topology requires the output voltage of the quasi-resonant control circuit to be connected in series with the input of the full-bridge inverter. In connection with this arrangement, the decreasing of the output voltage of the quasi-resonant control circuit (V_H) will result in the increasing of effective voltage across the full-bridge inverter. Consequently, the output voltage of the HV dc-dc converter is higher. This control scheme has drawbacks of complicated control strategy, which needs a complex control circuit. Moreover, the higher demand of switches and components leads to greater unwanted conduction loss, higher cost and bulkier size.

2.5.2 Parallel Resonant HV DC-DC Converter

A parallel resonant HV dc-dc converter uses all parasitic elements of HV transformer as resonant tank and does not require any additional external inductor or capacitor [50], [51]. In contrast to the series resonant converter, this topology as shown in Figure 2.12 has very good controllability at light load whereby the output voltage can be regulated over a wide range at no-load condition. However, the achievable range of output voltage reduced as the load increases. Therefore, it suffers from low controllability at heavy load condition [52], [53].

In addition, this topology is unable to prevent the saturation of HV transformer [52], [53]. The most critical problem of this topology is the non-proportioning between the resonant current and the load current. The resonant current will remain high even though the load decreases. Under this condition, the conduction losses are fixed, and thus diminish the efficiency at light load [32], [54], [55].

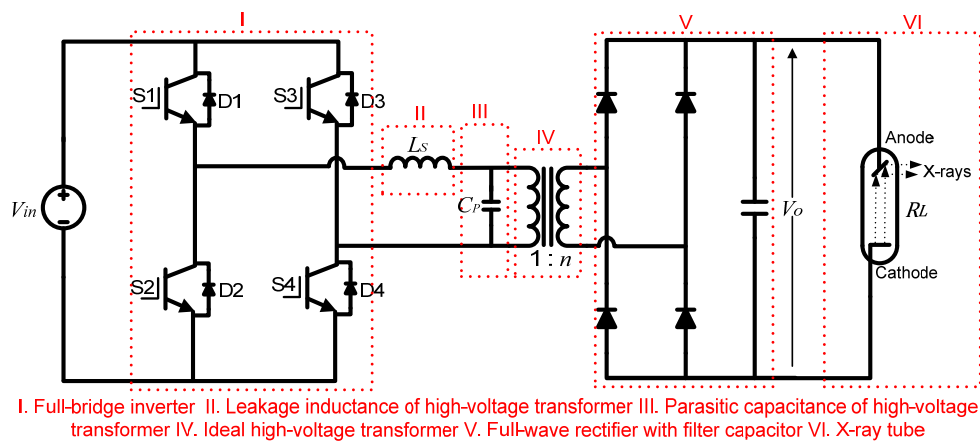


Figure 2.12: Parallel resonant HV dc-dc converter.

A parallel resonant HV dc-dc converter has two conduction modes as similar to the series resonant converter, namely DCM and CCM (below resonance or above

resonance) [56]. The soft switching condition of the full-bridge inverter switches in different conduction mode is described as follows: at both turn on and off in DCM [57], at turn off in CCM below resonance [57], and at turn on in CCM above resonance [58].

Generally, this topology is operated in CCM with the output voltage regulated by PSM [59]. However, the limitation of the output voltage range in heavy load condition makes PSM an imperfect control scheme [60]. Authors in [61] improved this topology by adding auxiliary resonant bridge-leg link snubbers in an attempt to achieve soft switching in all switches at both turn on and off. However, the number of switches and components are increased. In addition, the problems of controllability at heavy load and low efficiency at light load are unresolved.

2.5.3 Series-Parallel Resonant HV DC-DC Converter

The series-parallel resonant converter is often used along with inductive output filter [26], [30]. However, there are researchers employed it along with capacitive output filter [62], [63]. The capacitive output filter is suitable to be used in HV power supply for X-ray generator. Figure 2.13 shows the series-parallel resonant HV dc-dc converter. This topology uses both the leakage inductance and parasitic capacitance of HV transformer as resonant components with an externally connected capacitor in series with the transformer [64], [65].

With the assistance of the series capacitor in blocking the dc component, the saturation of HV transformer is avoided. Moreover, this topology takes advantage of both series and parallel resonant converter [32], [66]. The output voltage is able to be